AN APPLICATION OF PERSISTENT HOMOLOGY ON GRASSMANN MANIFOLDS FOR THE DETECTION OF SIGNALS IN HYPERSPECTRAL IMAGERY

Sofya Chepushtanova[1], *Michael Kirby*[1*], *Chris Peterson*[1], *Lori Ziegelmeier*[2]

[1]Department of Mathematics, Colorado State University, Fort Collins, CO, USA
[2]Department of Mathematics, Statistics, and CS, Macalester College, Saint Paul, MN, USA

ABSTRACT

We present an application of persistent homology to the detection of chemical plumes in hyperspectral movies. The pixels of the raw hyperspectral data cubes are mapped to the geometric framework of the real Grassmann manifold $G(k, n)$ (whose points parameterize the k-dimensional subspaces of $\mathbb{R}^n$) where they are analyzed, contrasting our approach with the more standard framework in Euclidean space. An advantage of this approach is that it allows the time slices in a hyperspectral movie to be collapsed to a sequence of points in such a way that some of the key structure within and between the slices is encoded by the points on the Grassmann manifold. This motivates the search for topological structure, associated with the evolution of the frames of a hyperspectral movie, within the corresponding points on the Grassmann manifold. The proposed framework affords the processing of large data sets, such as the hyperspectral movies explored in this investigation, while retaining valuable discriminative information.

Index Terms— Grassmann manifold, persistent homology, hyperspectral signal detection, subspaces, topological data analysis

1. INTRODUCTION

Hyperspectral imaging (HSI) involves the collection of detailed spectral information from a scene. A digital hyperspectral image can be considered as a three dimensional array consisting of two spatial dimensions and one spectral dimension. The spectral data consists of energy collected across tens to hundreds of narrow wavelength bands. Such images are called hyperspectral data cubes and are used in various hyperspectral data processing applications, e.g., material identification, land cover classification, or anomaly detection [1].

Including a temporal dimension in the process of data acquisition provides dynamic hyperspectral information in a 4-way array. Such a sequence of hyperspectral cubes collected at short time intervals is effectively a hyperspectral movie capturing potentially interesting spectral changes in a scene such as the release of a chemical plume. An important application of dynamic hyperspectral imaging is in the surveillance of the atmosphere for chemical or biological agents.

In this study, we consider an application of persistent homology (PH) to the detection of chemical plumes in hyperspectral imagery. PH is a relatively new tool in topological data analysis (TDA) that provides a multiscale method for analyzing the topological structure of data sets [2, 3]. The direct application of PH to large data sets, such as sequences of hyperspectral data cubes, can be prohibitive due to computational intractability. We overcome this issue by encoding the frames of a hyperspectral movie as points on a Grassmann manifold [4]. The real Grassmannian provides a paramterization of k-dimensional linear subspaces of $\mathbb{R}^n$, and a geometric framework for the representation of a set of raw hyperspectral data points by a single manifold point. This approach affords a form of compression while retaining pertinent topological structure. In this setting, it becomes feasible to utilize PH to analyze larger volumes of hyperspectral data as the high computational cost of PH applied to the original data space is greatly reduced.

We apply this approach to the detection of chemical signals in the collection of data cubes of the Long-Wavelength Infrared (LWIR) data set [5]. Using this framework, it is possible to generate topological signals that capture changes in the scene after a chemical release.

We organize the paper in the following order: Section 2 describes PH while the Grassmannian framework is explained in Section 3. Computational experiments are discussed in Section 4, followed by conclusions in Section 5.

2. PERSISTENT HOMOLOGY

Persistent homology is a computational approach to topology that allows one to answer basic questions about the structure of point clouds in data sets [2,3]. This procedure involves interpreting a point cloud as a noisy sampling of a topological space. Aspects of this topological space are uncovered by associating, to the data cloud, a nested sequence of simplicial complexes indexed by a scale parameter ϵ. Of particular interest are ϵ-dependent, kth order holes in the simplicial complexes, for these provide insight into the topological structure at different scales. For instance, zeroth order holes give the number of connected components (clusters) of the point cloud, while first order holes indicate the existence of topological circles, or periodic phenomenon. The connectivity of the simplicial complex may be viewed as arising from the overlapping of ϵ-balls that cover the data in the point cloud. As a result, these holes are a function of the scale ϵ. More formally, the number of kth order holes is the rank of the associated homology of the simplicial complex (also called the *kth Betti number*). In persistent homology, one seeks structures that persist over a range of scales. Thus, PH tracks homology classes of the point cloud along the scale parameter, indicating at which ϵ a hole appears and for which range of ϵ values it persists. The Betti numbers, as functions of the scale ϵ, can be visualized in a distinct barcode for each dimension k [6]. Note that in this paper, all of the information that is used to generate the PH barcodes for a point cloud is encoded in a matrix of pairwise distances between the points.

Figure 1 shows an example of the $k = 0$ and $k = 1$ barcodes generated for a point cloud sampled from the unit circle. Each horizontal bar represents the birth and death of a separate homology class, and the kth Betti number at any given parameter value ϵ is the number of bars that intersect the vertical line through ϵ. For the

*Email: kirby@math.colostate.edu

To appear in *Proc. IGARSS 2015, July 26-31, 2015, Milan, Italy*

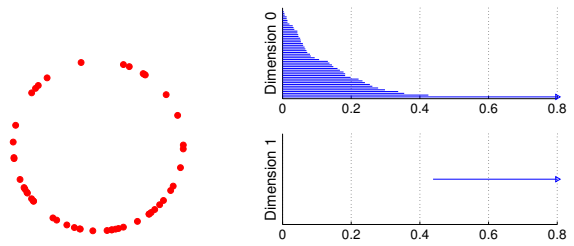

Fig. 1: $Betti_0$ (top right) and $Betti_1$ (bottom right) barcodes corresponding to point cloud data sampled from the unit circle (left).

circle, $Betti_0 = Betti_1 = 1$ which correspond to the number of connected components and number of loops, respectively, shown by the longest (persistent) horizontal bars in each plot. To generate the barcodes, we use JavaPlex, a library for persistent homology and topological data analysis [7]. In the next section, we discuss how PH can be used for HSI signal detection.

3. THE GRASSMANNIAN FRAMEWORK

We propose using the Grassmann manifold (Grassmannian) as a framework for detection of signals in hyperspectral imagery via PH. The real Grassmann manifold $G(k, n)$ parametrizes all k-dimensional subspaces of the vector space $\mathbb{R}^n$ [4]. A sequence of hyperspectral data cubes, or subcubes taken from them, can be mapped to points on $G(k, n)$. Figure 2 schematically illustrates the setting.

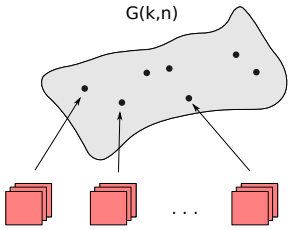

Fig. 2: A sequence of data cubes mapped to points on $G(k, n)$.

Note that if Y is a point on $G(k, n)$, it can be nonuniquely represented by an orthonormal basis U. Given a xyz-cube, one can reshape it into an $xy \times z$ matrix Y, whose columns span a subspace on $G(k, n)$ with $k = z$ and $n = xy$, provided $z < xy$. If we compute the reduced singular value decomposition (SVD) $Y = U\Sigma V^T$, the columns of the $n \times k$ orthogonal matrix U ($U^T U = I_k$) are a basis for the column space of Y. Thus, U can be used to represent the xyz-cube and can be identified with a point on the Grassmannian $G(k, n)$. Once the hyperspectral movie is mapped to a sequence of points on $G(k, n)$, the pairwise distances between these points may be found using an appropriate function of the angles between subspaces. For example, the chordal distance between k-dimensional subspaces $\mathcal{P}$ and $\mathcal{Q}$ is given by $d_c(\mathcal{P}, \mathcal{Q}) = (\sum_{i=1}^{k} (\sin\theta_i)^2)^{1/2} = \|\sin\theta\|_2$ and the geodesic distance is $d_g(\mathcal{P}, \mathcal{Q}) = (\sum_{i=1}^{k} \theta_i^2)^{1/2} = \|\theta\|_2$, where θ is the k-dimensional vector of the principal angles $\theta_i, i = 1, \ldots, k$, $0 \leq \theta_1 \leq \theta_2 \leq \ldots \leq \theta_k \leq \pi/2$, between $\mathcal{P}$ and $\mathcal{Q}$ [8,9].

In this paper, we measure the similarity of two points with the smallest principal angle, $d_p = \theta_1$, between the points. While not a metric, this nevertheless provides a useful tool for analysis [10, 11]. In fact, we observed in our experiments that using d_p resulted in stronger topological signals than did d_c and d_g. Once the sequence of cubes is mapped to $G(k, n)$, the matrix of all pairwise "distances" is computed, and we apply PH to generate $Betti_0$ barcodes to see the number of connected components (clusters) in the point cloud on the Grassmannian, corresponding to the raw HSI data.

4. EXPERIMENTAL RESULTS

In this section, we show results obtained by this approach applied to the detection of chemical signals in the collection of data cubes of the Long-Wavelength Infrared (LWIR) data set [5]. The LWIR data set is collected by an interferometer in the 8-11 μm range of the electromagnetic spectrum. During a single scanning, 256×256 pixel images are collected across 20 wavelengths within this range, forming a $256 \times 256 \times 20$ data cube. A single data collection event consists of releasing a pre-determined quantity of Triethyl Phosphate (TEP) into the air to create an aerosol plume for detection against natural background. A series of 561 data cubes records the entire event from "pre-burst" to "post-burst", as a hyperspectral movie.

To strengthen topological signals, the experimental setting includes dimension reduction of the band space, finding the patch in the images that contains the chemical cloud, mapping selected (sub)cubes to the Grassmannian, computing the pairwise distances on the manifold, and generating PH $Betti_0$ (or 0-dimensional) barcodes for clustering. Here we use 3 (out of 20) wavelength bands selected by the *sparse* support vector machine (SSVM) band selection algorithm, via classifying the TEP data points against the background points [12]. To validate our results we also determine the location of the plume in the cubes using the adaptive-cosine-estimator (ACE) [13].

4.1. Experiment on a Subset of Cubes

We first consider a subset of 561 TEP cubes: "pre-burst" cubes 104-111 and cubes 112-116, containing evolving plume. (Note that cube 112 is the cube in which a plume occurs for the first time.) To generate a $Betti_0$ barcode on these 13 cubes, a "plume location" patch of size $4 \times 8 \times 3$ from each cube is mapped to a point on $G(3, 4 \times 8) = G(3, 32)$. Figure 3 shows results of PH clustering over many scales. The 0-dimensional barcode in Figure 3a has different numbers of connected components as the scale parameter ϵ increases. For instance, at the small scale of $\epsilon = 5 \times 10^{-4}$, all the points are disconnected (13 bars are present), which is shown schematically in Figure 3b by distinct coloring for each point. Figure 3c depicts the clustering that occurs at $\epsilon = 4 \times 10^{-3}$. At this scale, we have 6 clusters, with one cluster containing all the "pre-burst" points 104-111 (shown in red), and 5 clusters each containing isolated plume points 112 to 116, indicated by distinct colors. Later, at $\epsilon = 6 \times 10^{-3}$, PH detects 3 clusters of points: plume points 112 and 113 join the cluster of points 104-111, and points 115 and 116 merge into a separate cluster, with point 114 staying isolated, see Figure 3d. This can be interpreted as follows: points 112 and 113, where the plume first develops, are closer to the "pre-plume" cluster on $G(3, 32)$ than the points 114, 115, 116, as the shape of the plume changes. In particular, PH tells us that each of the points within a cluster are are more similar on the manifold to other points within the cluster than to points not in the same cluster. When ϵ is large enough, all points merge into a single connected component.

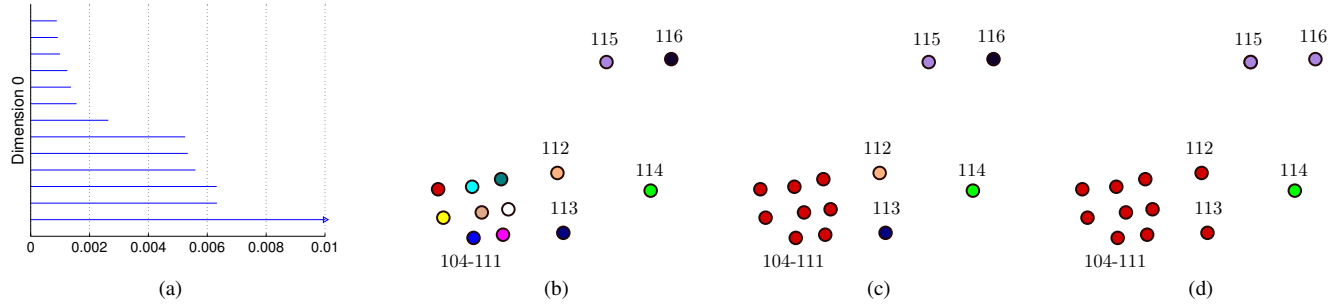

Fig. 3: (a) $Betti_0$ barcode generated on points on $G(3, 32)$, corresponding to $4 \times 8 \times 3$ subcubes 104 to 116 selected from 561 TEP data cubes; (b) 13 isolated points 104-116 on $G(3, 32)$ at $\epsilon = 5 \times 10^{-4}$, shown by distinct colors; (c) 6 clusters at $\epsilon = 4 \times 10^{-3}$: the red colored cluster of points 104-111 and 5 isolated points 112-116, shown by distinct colors; (d) 3 clusters at $\epsilon = 6 \times 10^{-3}$: the cluster of points 104-113 (red), the isolated point 114 (green), and the cluster of points 115 and 116 (purple).

4.2. Experiment on All Cubes

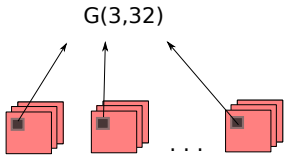

Fig. 4: Grassmannian setting for the 561 top (sky) left $4 \times 8 \times 3$ subcubes.

This experiment includes generating $Betti_0$ barcodes using all 561 TEP cubes. Similar to the experiment in Section 4.1, we consider $4 \times 8 \times 3$ subcubes "cut out" from different areas in each image such as the top (sky), the middle (horizon, where the plume develops), and the bottom (ground) for left, right, and center regions, respectively. See Figure 4 for an illustration of left subcubes from the sky mapped to $G(3, 32)$.

We generate nine 0-dimensional barcodes for the different regions described above, see Figure 5. Notice the similarity of the barcodes along the first (sky) and third (ground) rows, indicating uniformity in these regions throughout the hyperspectral movie. In contrast, the plume occurs and develops along the horizon. This dynamic movement within the scene is reflected in the fluctuation of the barcodes, see the second row in Figure 5.

Let us now further consider the clusters forming in the 0-dimensional barcode in Figure 5d. Recall that this barcode is generated from the 561 points corresponding to the left horizon $4 \times 8 \times 3$ region in each data cube, i.e., the plume formation region. At scale $\epsilon = 1.5 \times 10^{-3}$, there are 31 bars corresponding to 31 connected components on $G(3, 32)$, with 28 isolated points from frames 111 to 142, one cluster containing frames 134, 135, and 137, one cluster containing frame 519, and another containing all other frames. At scale $\epsilon = 2 \times 10^{-3}$, we have 19 bars corresponding to 19 connected components on $G(3, 32)$, with 18 isolated frames from 112 to 129, and one cluster containing all the rest. Note that these bars persist for a large range of parameter value (to just beyond 3×10^{-3}), indicating a large degree of separation. At $\epsilon = 4 \times 10^{-3}$, we have 13 clusters with 11 isolated frames 112-118 and 120-125, one cluster of frames 119 and 124, and the other one containing everything else.

Note that cubes following frame 111 are where the plume first occurs with the highest concentration of chemical and changes very fast. PH detects separation of these points from pre-plume cubes at multiple scales. The Grassmannian framework together with PH treats these points as far away from each other and from the rest of the points, therefore capturing the dynamics in the sequence of HSI images containing the chemical.

5. CONCLUSION

In summary, we presented a geometric framework for characterizing information in hyperspectral data cubes evolving in time. Persistent homology was employed to aid in detecting changes in topological structure on point clouds generated from raw HSI data under the Grassmannian framework. We observed that, depending on the PH parameter value ϵ, both all-cubes and subset-of-cubes experiments resulted in clustering that reflected the dynamical changes in the HSI sequences of cubes of the LWIR data set.

In the first experiment, with a small subset of Triethyl Phosphate cubes mapped to the Grassmannian, PH $Betti_0$ barcodes captured the evolution of the plume when it first occurred and started evolving. In the second, all-cubes experiment, different regions of the cubes were mapped to a manifold to generate barcodes. We observed changes in the barcode profiles obtained along the horizon ("plume") line, while the other regions in the cubes resulted in similar plots. Based on clustering results for the left horizon subcubes, several frames with a plume were treated by PH as isolated points on the manifold, in contrast to "pre-burst" points and points long after the release time, all clustered together.

Having found these results promising, further research can be done to strengthen the topological signal. We are working to employ other mappings, other (pseudo)metrics on the Grassmannian, and $Betti_1$ barcodes. We are further making a comparative analysis of no-plume and plume data cubes, based on mapping subsets of pixels to $G(1, n)$ where n is the number of spectral bands.

6. ACKNOWLEDGMENTS

The authors thank Henry Adams for providing MATLAB software for determining the indices of connected components in PH barcodes generated by JavaPlex.

This paper is based on research partially supported by the National Science Foundation (DMS-1228308, DMS-1322508) as well as the DOD-USAF (FA9550-12-1-0408). Any opinions, findings,

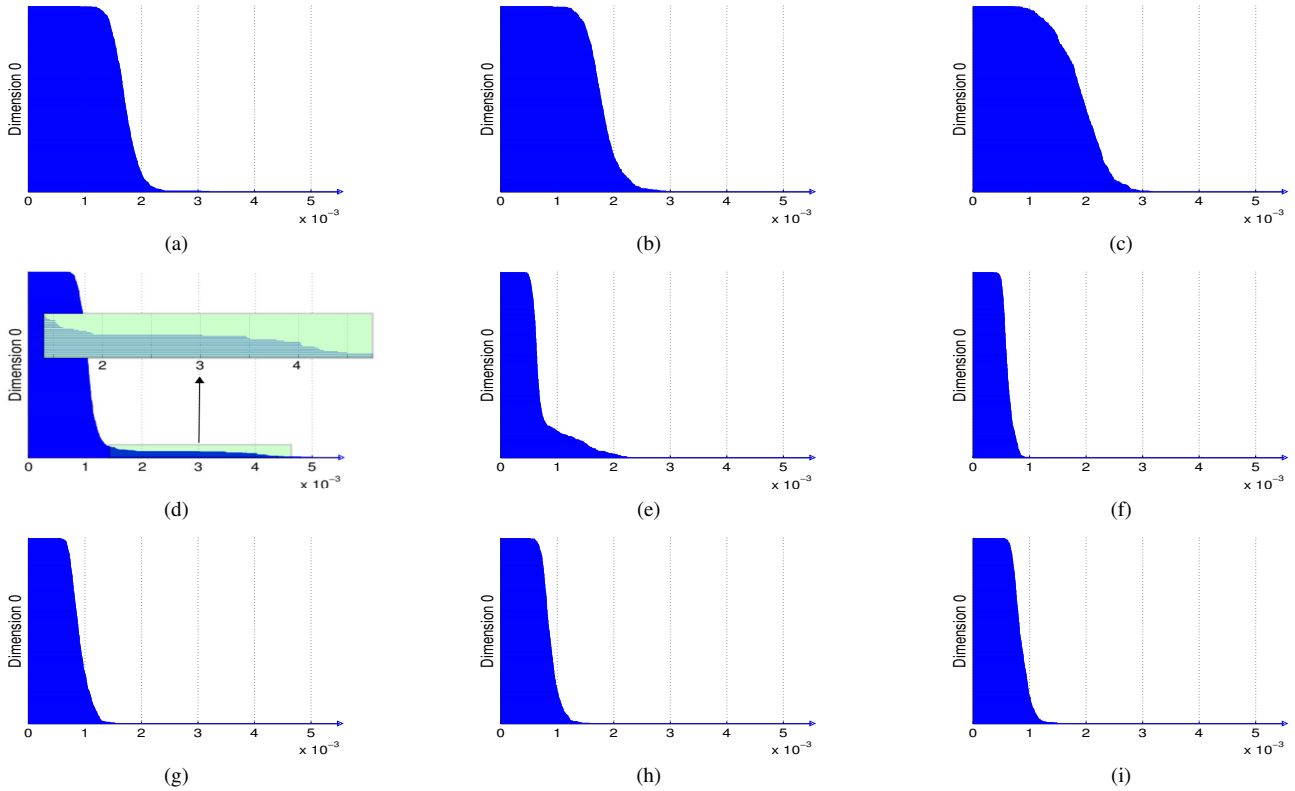

Fig. 5: $Betti_0$ barcodes generated on selected $4 \times 8 \times 3$ regions through all 561 TEP cubes, mapped to $G(3, 32)$: (a) top left; (b) top middle; (c) top right; (d) middle left; (e) center; (f) middle right; (g) bottom left; (h) bottom middle; (i) bottom right.

and conclusions or recommendations expressed in this material are those of the authors and do not necessarily reflect the views of the National Science Foundation or the United States Air Force.

7. REFERENCES

[1] David Landgrebe, "Hyperspectral image data analysis," *Signal Processing Magazine, IEEE*, vol. 19, no. 1, pp. 17–28, 2002.

[2] A. Zomorodian and G. Carlsson, "Computing persistent homology," *Discrete & Computational Geometry*, vol. 33, no. 2, pp. 249–274, 2005.

[3] H. Edelsbrunner, D. Letscher, and A. Zomorodian, "Topological persistence and simplification," *Foundations of Computer Science, 2000. Proceedings. 41st Annual Symposium on*, pp. 454–463, 2000.

[4] A. Edelman, T. A. Arias, and S. T. Smith, "The geometry of algorithms with orthogonality constraints," *SIAM J. Matrix Anal. Appl.*, vol. 20, no. 2, pp. 303–353, 1998.

[5] B. R. Cosofret, D. Konno, A. Faghfouri, H. S. Kindle, C. M. Gittins, M. L. Finson, T. E. Janov, M. J. Levreault, R. K. Miyashiro, and W. J. Marinelli, "Imaging sensor constellation for tomographic chemical cloud mapping," *Applied Optics*, vol. 48, pp. 1837–1852, 2009.

[6] R. Ghrist, "Barcodes: The persistent topology of data," *Bulletin of the American Mathematical Society*, vol. 45, pp. 61–75, 2008.

[7] A. Tausz, M. Vejdemo-Johansson, and H. Adams, "JavaPlex: A research software package for persistent cohomology," in *Proceedings of ICMS 2014*, Han Hong and Chee Yap, Eds., 2014, Lecture Notes in Computer Science 8592, pp. 129–136.

[8] Å. Björck and G. H. Golub, "Numerical methods for computing angles between linear subspaces," *Mathematics of Computation*, vol. 27, no. 123, pp. 579–594, 1973.

[9] J. H. Conway, R. H. Hardin, and N. J. A. Sloane, "Packing lines, planes, etc.: packings in Grassmannian spaces," *Experimental Mathematics*, vol. 5, pp. 139–159, 1996.

[10] J.-M. Chang, M. Kirby, H. Kley, C. Peterson, B. A. Draper, and J.R. Beveridge, "Recognition of digital images of the human face at ultra low resolution via illumination spaces," *ACCV*, vol. II, pp. 733–743, 2007.

[11] S. Chepushtanova and M. Kirby, "Classification of hyperspectral imagery on embedded Grassmannians," in *Proc. of the 2014 IEEE WHISPERS Workshop*, Lausanne, Switzerland, june 2014.

[12] S. Chepushtanova, C. Gittins, and M. Kirby, "Band selection in hyperspectral imagery using sparse support vector machines," in *Proc. SPIE*, 2014, vol. 9088, pp. 90881F–90881F–15.

[13] D. Manolakis, "Signal processing algorithms for hyperspectral remote sensing of chemical plumes," in *Acoustics, Speech and Signal Processing, 2008. ICASSP 2008. IEEE International Conference on*, March 2008, pp. 1857–1860.